Rydberg-electron decoherence in experimentally obtained recurrence spectra

M. L. Keeler, W. Setzer, and W. W. Martin
Physics Department, University of Minnesota–Morris, Morris, Minnesota 56267, USA
(Received 13 September 2010; published 8 November 2010)

Using scaled-energy spectroscopy techniques (recurrence spectroscopy) we investigate the influence of collisionally induced decoherence on semiclassical orbits in the Stark-Rydberg system. This experimental investigation represents the first application of recurrence spectroscopy to an atomic system perturbed by collisions with external gas partners. We present high-resolution recurrence spectra of potassium, revealing core-scattered combination orbits, and with minor modifications to the data acquisition process, recurrence spectra were also obtained with the system perturbed by 10 torr of krypton gas. A simple decoherence model is applied to semiclassical theory to explain the loss of recurrence strength at high actions. In several cases we also observe the loss of coherent interference *between* orbits. The loss of coherent destructive interference causes an increase in the recurrence strength of several core-scattered combination orbits.

DOI: 10.1103/PhysRevA.82.053406 PACS number(s): 32.80.Ee, 34.80.Pa, 32.70.Jz, 32.60.+i

I. INTRODUCTION

Fourier transform spectroscopy of Rydberg atoms is a well-established means for investigating the classical trajectories of excited electrons. Fourier components of an energy spectrum return classical orbit periods, whereas the transform of a scaled-energy spectrum reveals classical orbit actions [1–3]. For Rydberg systems in the presence of external electric or magnetic fields, acquisition of the absorption spectrum while maintaining a constant scaled energy permits a semiclassical analysis on a wide range of dynamical orbit types [4–6]. This experimental technique is known as recurrence spectroscopy and has been applied to numerous atomic systems in both electric and magnetic fields [7–18]. As an investigative tool it has revealed the existence of unique "combination orbits" or hydrogenic orbits that are connected through an elastic collision with the remaining core electrons [7,9]. In recent work by Wright *et al.* [19] recurrences in the scaled-absorption spectrum of H_2 are interpreted as inelastic collisions with the molecular core. Recurrence spectroscopy and semiclassical theory have also been applied to *externally* perturbed systems, including rf fields and the fields of nearby conducting surfaces [20,21]. This represents a study in which scaled-energy analysis is applied to Rydberg atoms perturbed by collisions with external partners. Specifically we take recurrence spectra of potassium Rydberg atoms in a Stark field while in a bath of krypton gas. With the introduction of a background gas we expect line shift, line broadening, and state mixing. We accommodate the line shift and interpret variations in recurrences in terms of semiclassical decoherence.

Recurrence spectroscopy of Rydberg atoms in an external electric field is based on a scaling of the classical Hamiltonian. In atomic units the Hamiltonian for the excited electron,

$$H = \frac{p^2}{2} - \frac{1}{r} + F_Z, \tag{1}$$

can be replaced with a set of scaled variables such that

$$\tilde{H} = \varepsilon = \frac{E}{\sqrt{F}} = \frac{\tilde{p}^2}{2} - \frac{1}{\tilde{r}} + \tilde{z}. \tag{2}$$

Here the new scaled Hamiltonian, $\tilde{H}$, is independent of the external field. Thus, if the scaled energy, ε, is held constant, the classical dynamics remains unchanged [1]. If the energy of the excitation laser (E) is increased and the external field (F) is simultaneously changed to maintain a constant scaled energy (ε), then each bound orbit, independent of launching angle, is scaled up in size. Semiclassical closed-orbit theory (COT) suggests that an individual closed, classical orbit contributes a specific frequency to the scaled-absorption spectrum or absorption as a function of the scaled parameter w [5]:

$$w = F^{-1/4} = \sqrt{\varepsilon/E}. \tag{3}$$

In the semiclassical model of COT, outgoing wave fronts associated with the initial laser excitation are propagated via classical trajectories. These trajectories return to the core, producing a coherent returning wavefront that interferes with the original outgoing wave front. As these orbits are expanded in size (increasing laser energy while maintaining a constant scaled energy ε), the continuously increasing phase of the returning wave front produces a regular interference with the outgoing wave front and consequently an oscillation in the absorption spectrum. In experimental recurrence spectroscopy a scaled-absorption spectrum is acquired at a constant ε, and the Fourier transform isolates the frequency components associated with individual closed orbits. Peak height in the recurrence spectrum (recurrence strength) reflects the initial orbit launching probability, the classical orbit stability, and the interference between orbits returning to the core.

For sufficiently high values of n, collisional line shift has been shown to be independent of n [22–25]. The dynamical information in a scaled-absorption spectrum is contained within the frequencies of that spectrum, and a constant shift does not alter those frequencies or the fundamental dynamics. During recurrence spectroscopy data collection, the external field is modified to maintain a constant scaled energy:

$$F = (E/\varepsilon)^2. \tag{4}$$

Here E is the binding energy and F is the external field strength. As gas is added to the system spectral lines are shifted to deeper binding energies, or further from ionization.

Experimentally the average spectral shift (Δ in atomic units) is measured just prior to the acquisition of recurrence data where the applied field is modified accordingly:

$$F = \left(\frac{E+\Delta}{\varepsilon}\right)^2. \quad (5)$$

II. UNPERTURBED RECURRENCE SPECTRA

A. Experimental apparatus

The apparatus, essentially a thermionic diode, has been described in a previous publication [17]. A vacuum chamber (maintained around 170°C) is filled with potassium vapor where a two-photon excitation is used to generate potassium Rydberg atoms. For our current experimental arrangement we estimate the density of potassium vapor to be about 2×10^{13} atoms/cm^3. The first photon (405 nm, polarized parallel to the electric field) is generated using a cavity-stabilized Sanyo 5-mW laser diode and excites ground-state potassium atoms to the $5p_{3/2}$ state. A second infrared photon ($\lambda = 974$–978.5 nm), generated from a commercially available tunable laser diode, excites from the $5p_{3/2}$ state to Rydberg states of the range $n = 40$–70. Excitation occurs between two Stark plates (approximately 30 cm long, 1 cm separation), one of which serves to detect the ions resulting from collisionally ionized Rydberg atoms. The relatively high gas-density and short mean-free path prevents secondary emission or amplification via cascading ionization. We mechanically chop the infrared laser and use a lock-in amplifier to measure currents on the order of 100 pA. The laser wavelength calibration and line-shift measurement is accomplished by acquiring an absorption spectrum at a field strength of 0.175 V/cm. During the acquisition of a recurrence spectrum the laser wavelength is continuously scanned and monitored by a computer that, in real time, updates the electric field according to Eq. (5). The raw data is then interpolated to create a data set equally spaced with respect to the independent parameter w [Eq. (3)]. We square the Fourier transform of this scaled-absorption spectrum to obtain the recurrence spectrum, a plot of recurrence strength versus scaled action. Multiplying the scaled action by $\sqrt{-2\varepsilon}$ produces a recurrence map where orbits of a constant period ratio generally fall on integer or half-integer scaled-action values [11]. *All references to scaled action in this article have assumed this multiplicative factor.* Recurrence spectra are taken as a function of scaled energy and assembled into a three-dimensional recurrence map. Specific orbits are generally identified by their period ratio as computed in semiparabolic coordinates [26]. Explanations of the general features and structures found within recurrence maps can be found in Refs. [9–11,26–28]. Courtney *et al.* [7] found and identified the experimental evidence for core-scattered "combination orbits" which are not found in hydrogen. In combination orbits the returning electron scatters off the core electrons into another closed orbit. The scaled action of the resulting orbit is the sum of the actions of the parent orbits. Figure 1 shows two experimentally obtained recurrence maps of potassium with some orbits identified, including several combination orbits. We would like to note that because of the relatively large range of quantum numbers spanned that our resolution in scaled action is high (<0.04), and this allows for the unique opportunity to resolve these combinations.

B. Polarization and recurrence strength distributions

The first map of Fig. 1 was taken with the infrared laser polarization oriented parallel to the electric field, whereas the second map was taken with the perpendicular polarization. Selection rules for small atoms dictate that light polarized parallel to the field allow $\Delta m_l = 0$, and for light polarized perpendicular to the field $\Delta m_l = \pm 1$. Our intermediate state, $5P^{3/2}$, $|m_j| = 1/2$, has both $m_l = 1$ and $m_l = 0$ components, and based on these simple rules, excitation using light polarized perpendicular to the external field produces a coherent mixture of $m_l = 0$, 1, and 2 components. From semiclassical COT, the laser polarization determines the initial launching angle distribution of the electron. This initial distribution can be found by applying the dipole operator to the initial state as described in the work of Gao and Delos [6].

These initial launching distributions (Eq. (5.16) of Ref. [6] and Eq. (60.2-60.11) of Ref. [29]) are *partially* responsible for the distribution of strengths mapped out in Fig. 1, as the initial launching angle can be mapped to scaled energy for a given orbit. However, because of other contributions to recurrence strength, these distributions are not easily seen in the recurrence strength profiles of Fig. 1. It has been noted that in the case of nonhydrogenic atoms, core-scattered combination orbits occurring at actions near hydrogenic orbits will interfere and significantly alter an apparent orbit profile [9,11,27]. We chose to focus our investigations on the perpendicular polarization because of the *apparent* variety of orbits observed in our experimental data.

III. PERTURBED RECURRENCE SPECTRA

Prior to taking recurrence spectra in the presence of krypton gas we obtained field-free absorption spectra. With the addition of krypton gas we observed spectral line broadening and line shifts on the order of 140 and 630 MHz/torr, respectively (Fig. 2). In the field-free case (fields less than 200 mV/cm), a second Rydberg series associated with the $5p_{1/2}$ state appears. Collisional deexcitation from the intermediate $5p_{3/2}$ state populates the $5p_{1/2}$ state leading to a statistical mixture of the two. The final absorption spectrum is therefore composed of the incoherent excitation of two Rydberg series separated by approximately 20 cm^{-1}. The second series becomes apparent with the addition of tens of millitorr and grows stronger with higher gas pressures. The relative strength of the series originating from the $j = 1/2$ state becomes comparable with the $j = 3/2$ state and saturates when the gas pressure exceeds a few torr.

The admixture of the two Rydberg series would appear to make meaningful recurrence spectroscopy difficult, but the specific scaling of Eq. (5) is "tuned" to one set of energies, and in this case the Fourier transform preferentially extracts recurrences tied to the $5p_{3/2}$-ns,p series. In addition, we identify artifacts in the recurrence spectrum due to this second series by repeating the experiment under low gas conditions

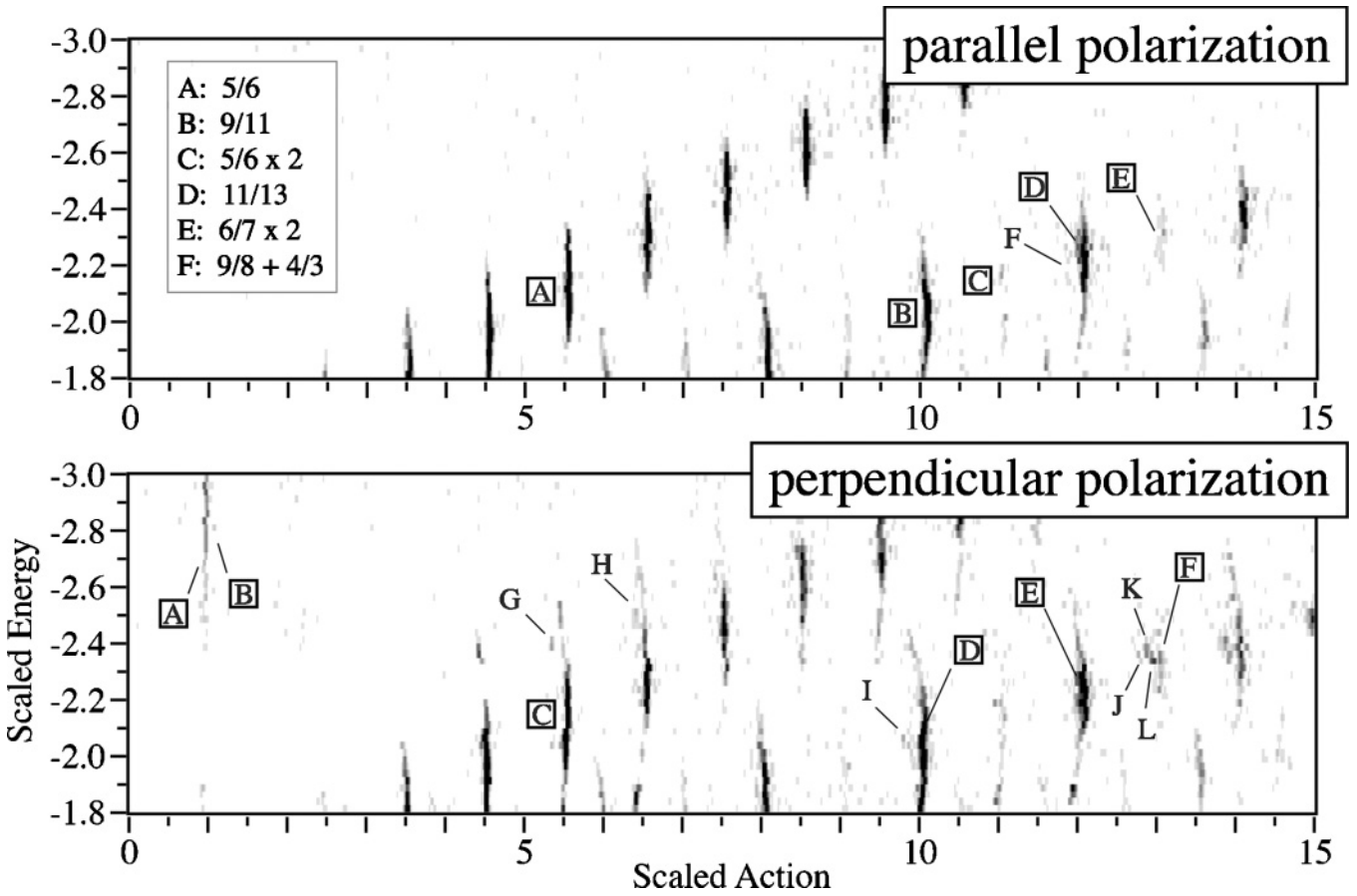

FIG. 1. Recurrence maps for infrared light polarized parallel and perpendicular to the electric field. Darker regions are regions of higher recurrence strength, or orbit probability, with the gray scale spanning one decade. The orbit legend for the parallel polarization is contained within the top map. Apparent hydrogenic orbits are labeled (boxed labels) by their period ratio in semiparabolic coordinates (u/v), and orbit repetitions are indicated by "xj" where j is the repetition number (a primitive uphill or downhill repetition is indicated with uj or dj). Nonhydrogenic combination orbits are indicated by the parent orbits separated by an addition symbol. The orbit identification for the perpendicular polarization map is as follows (with unresolved orbits separated by commas and nonhydrogenic combinations in bold): A = primitive uphill; B = primitive downhill; C = 5/6; D = 9/11, **5/6 + 4/5**; E = 11/13; F = 6/7 × 2, **11/13 + d**; G = **4/5 + u**, **d4 + u**; H = **5/6 + u**, **d5 + u**; I = **7/8 + d2**, **7/9 + d2**; J = **9/10 + d3**, **9/11 + u3**; K = **8/9 + 4/5**; L = **7/8 + 5/6**, **11/13 + u**.

while selectively tuning the first laser to the $5p_{1/2}$ state. A recurrence spectrum taken under these conditions points to regions within the recurrence map where we know artifacts will reside. Unfortunately this treatment assumes that the two spectra are isolated. At certain points within the scaled-absorption spectrum, frequencies within the $j = 1/2$ series may interfere constructively or destructively with those of the $j = 3/2$ series. We can predict these effects by adding the "pure" laser-excited $j = 3/2$ and $j = 1/2$ scaled-absorption spectra prior to taking the Fourier transform. We use this technique to positively confirm that unique features of the gas-perturbed recurrence map are in fact due to collisions between the Rydberg electron and krypton gas, as opposed to the $j = 1/2$ Rydberg series.

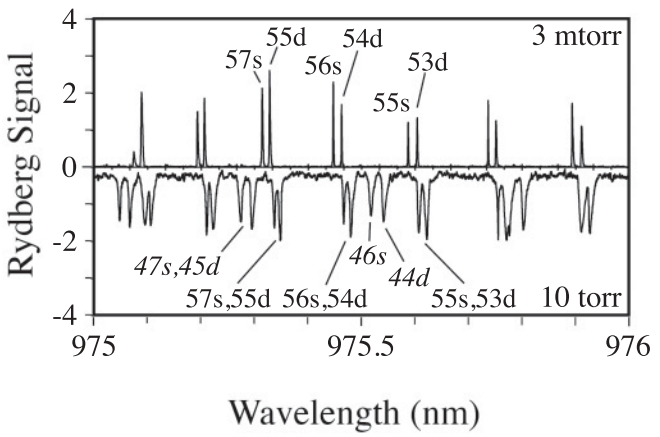

FIG. 2. Field-free absorption spectrum taken at low and high gas pressures. Peak assignments associated with the series originating from the $5p_{1/2}$ state are identified with an italic font.

Scaled-absorption spectra were acquired according to Eqs. (3) and (5) from $\varepsilon = -1.9$ to $\varepsilon = -2.85$ in increments of -0.025 and transformed into recurrence spectra. Each recurrence spectrum was normalized to the integral of the strength over the region $\tilde{S} = 1 \rightarrow 50$. This accounts for daily fluctuations in signal strength while minimizing the influence of the $5p_{1/2}$ series whose contributions are concentrated at scaled actions less than 1. The normalized recurrence spectra were assembled into maps similar to those of Fig. 1.

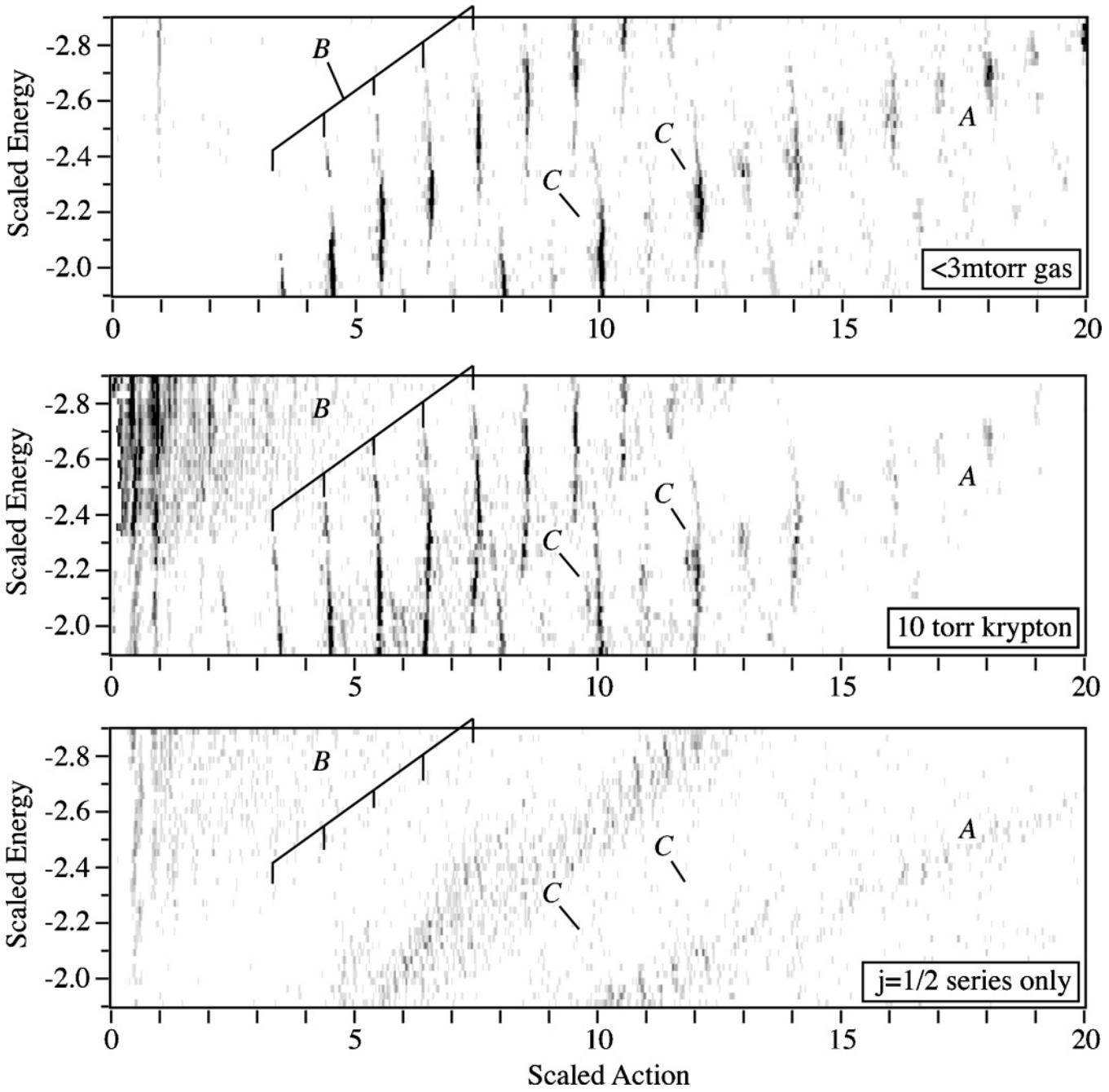

FIG. 3. A comparison of recurrence maps with low and high levels of background gas. The third map identifies artifacts from the $j = 1/2$ Rydberg series. Letters identify locations where key differences can be found between the maps.

Figure 3 compares recurrence maps with low and high levels of background gas. The last map of Figure 3 shows recurrence spectra taken with just the $5p_{1/2}$ series present. Select points where the maps differ are indicated with letters. For example, the area indicated by A has a much lower recurrence strength in the 10 torr krypton map. This is primarily due to collisional decoherence of the electron wave front returning to the core. In our analysis we intentionally investigate features where there is little possibility of interference from the $5p_{1/2}$ spectrum. The remainder of this article is devoted to explaining the features pointed out in Fig. 3 in terms of collisional decoherence.

IV. RYDBERG-ELECTRON NOBEL GAS COLLISIONS AND DECOHERENCE

A. General considerations

Fermi approached the problem of Rydberg-electron noble gas collisions with an independent particle model and the idea of a simple pseudopotential [22]:

$$V(r) = 2\pi L|\psi(r)|^2, \tag{6a}$$

$$\sigma_{\text{scatt}} = 4\pi L^2. \tag{6b}$$

Here L is known as the scattering length. In a purely classical picture the scattering rate is given by the average electron

velocity multiplied by the scattering cross section. Given that the average velocity is the orbit path length divided by the orbit period we find that the number of scattering events is proportional to the classical (round-trip) orbit length:

$$N_{\text{events}} = 4\pi L^2 \langle l_{\text{orb}} \rangle N_p. \tag{7}$$

For example, for a classical low-angular momentum orbit at $n = 55$ in a bath of krypton gas ($L = 3.7$, $N_p = 1/760$), we expect approximately 2740 scattering events/torr/orbit.

From Eq. (7) we expect longer orbits to experience more scattering and a reduction in recurrence strength. At higher field strengths (near ionization threshold, $\varepsilon = -2$), a downhill oriented orbit becomes significantly stretched by the external field and is more vulnerable to scattering effects than an uphill-oriented orbit with an identical scaled action. Numerical integration of the equations of motion show that at $\varepsilon = -2.02$ (just below the ionization threshold), we expect a downhill-oriented primitive orbit to experience twice as many scattering events as an uphill primitive orbit. Then for high fields, all scattering effects will be more pronounced for classical orbits launched in the downhill direction.

At values of high n the electron momentum is low enough such that s-wave scattering dominates, and the short scattering length implies a small scattering amplitude. The forward-scattered component adds coherently to the unscattered wave front to produce a net phase shift. Many such scattering events accumulate to produce a spectral line shift, and statistical variations in the number of scattering events lead to spectral line broadening. The statistical variation in the returning phase due to scattering can also be interpreted as irreversible decoherence.

B. Line broadening and decoherence

There are three classical mechanisms that contribute to line broadening: elastic and inelastic collisions between the Rydberg electron and the perturber, and scattering between the ionic core and the perturber. For potassium Rydberg atoms in a bath of krypton we expect about equal contributions from elastic and inelastic collisions, for a total line broadening of about 124 MHz/torr [23]. Allard *et al.* [24] applied a statistical analysis to extend this model to higher gas densities and predicts a Gaussian line shape that grows in width as the square root of the gas density. Our measurements at 10 torr show a broadening rate of about 140 MHz/torr, comparable to the broadening rate predicted by Omont [23].

Scaled energy spectroscopy relies on the ability to resolve frequencies in the scaled-absorption spectrum. Line broadening will have the immediate effect of limiting the resolution of high frequencies which, through the power spectrum, are directly mapped to orbits with high action. We can quickly estimate the effects of line broadening on peaks within the recurrence spectrum by assuming a Gaussian line shape.

A Gaussian peak in the scaled-absorption spectrum $\chi(w)$ generates a Gaussian envelope in the power spectrum which attenuates high-action orbits. The attenuation of the recurrence spectrum $P(\tilde{S})$ can be written in terms of the original full width at half maximum (FWHM) linewidth in the scaled-absorption spectrum α:

$$\chi(w) = e^{-4\ln(2)w^2/\alpha^2}, \tag{8a}$$

$$P(\tilde{S}) = e^{-\tilde{S}^2\alpha^2/8\ln(2)}. \tag{8b}$$

The effective linewidth (α) in the scaled-absorption spectrum (w spectrum) can be approximated, $\Delta w = \Delta E_{\text{line}} \bar{n}^3$, in which case the expressions for the attenuating envelope and corresponding FWHM (β) are

$$P(\tilde{S}) = e^{-\tilde{S}^2\Delta E^2 n^6 \pi^2/2\ln(2)}, \tag{9}$$

$$\beta \cong 2/(\pi \Delta E_{\text{line}} n^3). \tag{10}$$

With a spectral linewidth of 1400 MHz (typical for 10 torr) and our average n value (55), the FWHM of the attenuating envelope is about 18. Then we would expect the recurrence strength for a peak located at a scaled action of 18 to be reduced to half of its original strength with the introduction of 10 torr of gas. Orbits higher in action would be even further attenuated.

The preceding analysis is based solely on the mathematical recipe for obtaining a recurrence spectrum and fails to provide physical interpretation. An alternative approach to modeling the effects of line broadening in recurrence spectra is to describe the collisional decoherence of semiclassical orbits. That line broadening is independent of n implies that the phase uncertainty of a wave front returning to the core has an n^3 dependence:

$$\delta/2_{\text{scatt}} \cong 2\pi n^3 \Delta E_{\text{line}}. \tag{11}$$

Physically this is because the number of interacting scatterers is proportional to the classical period of the Rydberg orbit, $\tau = 2\pi n^3$,

$$\delta/2_{\text{scatt}} \cong \tau \Delta E_{\text{line}}. \tag{12}$$

As in optics, fringe visibility due to temporal decoherence is quantified by the magnitude of the correlation function (perfectly coherent $\gamma = 1$, incoherent $\gamma = 0$),

$$|\gamma| = 1 - \tau/\tau_0, \tag{13}$$

where τ_0 is the coherence time. Using Eq. (12) and defining the coherence time as the time required to accumulate a 2π phase shift, we obtain a general expression for fringe visibility of a classical orbit with period τ:

$$|\gamma| = 1 - \tau \Delta E_{\text{line}}/2\pi. \tag{14}$$

Noting that the energy spacing between adjacent Rydberg states is proportional to n^{-3} (ΔE_R) we can write the correlation function in terms of energy rather than time:

$$|\gamma| = 1 - \tau \Delta E_{\text{line}}/\Delta E_R. \tag{15}$$

Clearly, if the characteristic linewidth is comparable to line separation, then coherence is lost.

Equation (13) is a general expression that predicts variation in decoherence losses with orbit period. In contrast, the simple spectral analysis of Eq. (9) predicts the same attenuating envelope, independent of the scaled energy and orbit launching angle. To directly compare models we can apply the semiclassical decoherence model to a field-free hydrogenic recurrence spectrum consisting of primitive orbits and their repetitions which occur at integer actions. In this case orbit periods

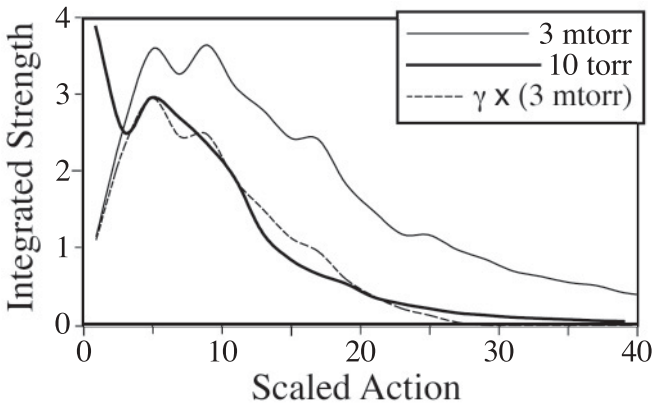

FIG. 4. Integrated recurrence strength versus scaled action. The dashed line is the result of applying a simple decoherence model [Eq. (16)] to the 3 mtorr data.

are directly correlated to their actions, $\tau = 2\pi \tilde{S} n^3$, and the envelope describing decoherence loss is

$$|\gamma| = 1 - \Delta E_{\text{line}} \tilde{S} n^3. \tag{16}$$

This simplified version of Eq. (13) assumes that all orbit periods are simply proportional to their scaled action, which is not the case in the presence of an external field. Nevertheless, for our experimental linewidth and average n value, Eq. (16) predicts $\gamma = 0.5$ and a 50% drop in recurrence strength at a scaled action of 14.11. This is in rough agreement with the predictions from Gaussian line broadening (9) and the recurrence maps of Fig. 3, area labeled A.

To directly compare our data with Eq. (16), we effectively average out the influences of the external field by integrating the recurrence strength over the scaled energy. Strips of data, $\Delta\tilde{S} = 2$, centered at odd-numbered actions were integrated over the full range of scaled energies to give a general picture of how the recurrence strength varies with scaled action. Figure 4 compares the results of this integration for the recurrence maps with 3 mtorr and 10 torr of gas. We apply Eq. (16) to the 3 mtorr data and see that this model of decoherence reasonably predicts the recurrence strength distribution of the 10 torr data. This simple model does differ from the Gaussian broadening model in that it predicts a hard "cutoff" when the classical period is equal to the coherence time, after which the recurrence strength becomes zero.

C. Influence of decoherence on orbit-orbit interference

Using the semiclassical picture adopted in COT, an isolated orbit is launched from the core, propagates classically, and then returns to the core to interfere with itself. In the previous section a simple theory of collisional decoherence is applied to isolated orbits, and the failure of an orbit to interfere with itself predicts a loss in the observed recurrence strength. But COT allows for the simultaneous launching of all orbits that interfere not only with themselves but also with each other. We then predict that in instances where two orbits are interfering constructively, the addition of gas reduces coherency and recurrence strength is lost. Conversely, if two orbits are *destructive*, the addition of a perturbing gas would again reduce the level of coherence and actually *increase* the recurrence strength in the vicinity of these orbits. Gao and Delos [5,6] describe how a recurrence spectrum can be constructed from the coherent sum of semiclassical orbits:

$$R(\tilde{S}) = \left[\sum_j D_j \frac{\sin(a x_j)}{a x_j}\right]^2. \tag{17}$$

Here R is the recurrence strength resulting from the coherent addition of j orbits with strength D_j, where (with our modified definition of scaled action)

$$x_j = \tilde{S}_j - \tilde{S}, \tag{18a}$$

$$D_j = C_j e^{(b\tilde{S}_j - \phi_j)}, \tag{18b}$$

$$a = \pi(n_2 - n_1), \tag{18c}$$

$$b = \pi(n_2 + n_1). \tag{18d}$$

Equation (17) predicts a sinc^2-shaped peak for the recurrence strength of isolated orbits, where the classical scaled action is $\tilde{S}_j$ and (ignoring the initial launching angle distribution) C_j is the classical stability. We can expand this sum for two orbits (subscripts 1 and 2) and include γ to describe the system as a function of the degree of coherence (γ):

$$R(\tilde{S}) = \gamma_1 \left[\frac{D_1 \sin(a x_1)}{a x_1}\right]^2 + \gamma_2 \left[\frac{D_2 \sin(a x_2)}{a x_2}\right]^2 + \gamma_1\gamma_2 \frac{D_1 D_2 \sin(a x_1)\sin(a x_2)}{a^2 x_1 x_2}. \tag{19}$$

As opposed to the decoherence losses of an isolated orbit, the effect of decoherence with respect to two interfering orbits is cumulative. This is physically justified by the fact that the returning wave fronts of two different classical orbits both experience collisional decoherence, as opposed to an electron interfering with itself where the outgoing wave front presumably starts in a highly coherent state.

As noted earlier, the interference of hydrogenic and combination orbits can significantly modify orbit profiles, and the features indicated by B in Fig. 3 are presumably due to the interference between several orbits. To better illustrate differences between the maps in these areas we extract orbit profiles from the data of Fig. 3. Sections of recurrence map are integrated around the locations of hydrogenic orbits with a constant period ratio. For example, the 4/5 orbit profile is the integrated recurrence strength from scaled action 4.38 to 4.62 as a function of scaled energy. We naively identify and label orbit profiles by the dominant hydrogenic contributor, but acknowledge that there are certainly other hydrogenic and nonhydrogenic orbits that contribute to the recurrence strengths within a given profile. Figure 5 shows the orbit profiles associated with the feature labeled B in Fig. 3.

Even with some uncertainty in the absolute normalization of the recurrence strength the profiles (Fig. 5) show that the "downhill" side of these orbits (more negative scaled energy) experience an increase in strength relative to the orbit "center" where the launching angle is perpendicular to the external field. (Orbit centers of the 4/5, 5/6, and 6/7 orbits occur at $\varepsilon = -1.92$, 2.15, and 2.25, respectively.) In addition, by combining the unperturbed spectra excited from the $5p_{3/2}$ and

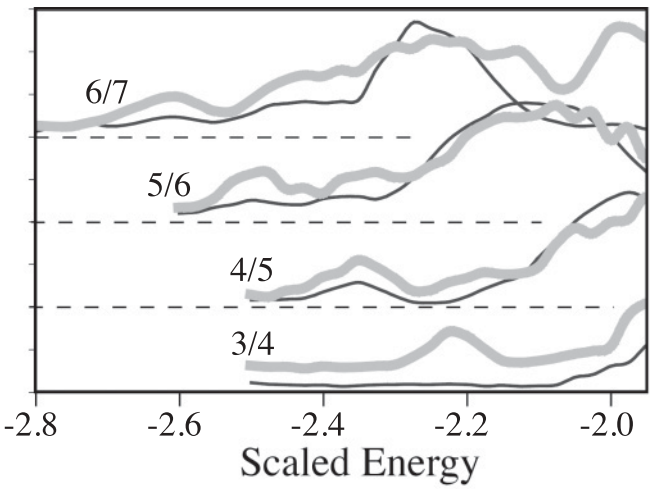

FIG. 5. Narrow strips of recurrence map integrated around regions containing a hydrogenic orbit are known as orbit profiles. The 3/4, 4/5, 5/6, and 6/7 orbit profiles are shown with vertical offsets indicated by dashed horizontal lines. The thin dark lines are the profiles taken from the 3 mtorr recurrence map while thick gray lines are the profiles taken from the 10 torr map.

$5p_{1/2}$ states we confirmed that accidental resonances between these series could not account for the observed increase in strength.

There are several orbits contributing to the 5/6 and 6/7 recurrence profiles. Figure 6 shows the locations of the most important orbits in these regions. Within close proximity to the downhill bifurcation point the primary hydrogenic orbit (5/6) interferes with the hydrogenic downhill repetition ($d5$). For potassium, a combination orbit formed by the neighboring hydrogenic orbit and primitive downhill also passes near this region ($4/5 + d$). Finally, a pair of combination orbits

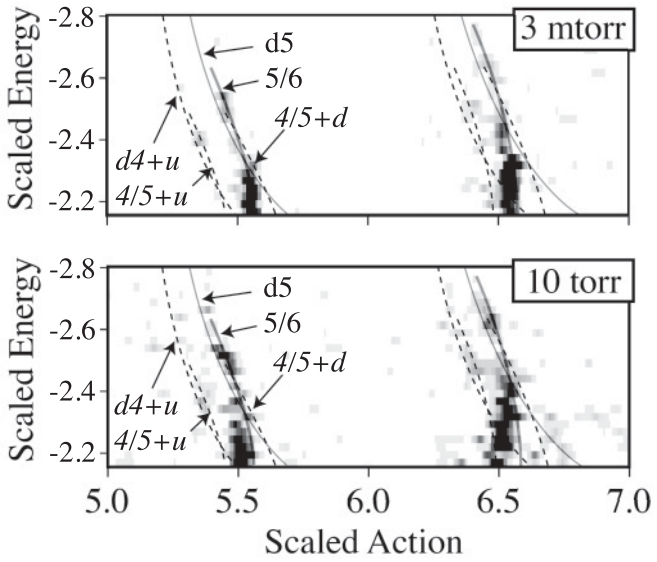

FIG. 6. Sections of recurrence map centered around the 5/6 and 6/7 hydrogenic orbits with the most important contributors identified (solid lines are hydrogenic; dashed lines are combination orbits).

($d4 + u$ and $4/5 + u$) are responsible for the small features occurring at slightly lower actions, also identified as H in Fig. 1. These patterns repeat themselves for the 6/7 profile. In the 3 mtorr data the lack of strength on the downhill side of these orbit profiles suggests that the $i/j + d$ combination orbit is destructive with the hydrogenic i/j orbit. Likewise, the ($d4 + u$) and ($4/5 + u$) pair are largely destructive with some recurrence strength appearing where the two classical actions separate slightly. These instances of destructive interference are reduced in the presence of collisional decoherence, as seen in the 10 torr map of Fig. 6. Using Eq. (13) we can estimate γ for the 5/6 and $4/5 + d$ orbits and find the reduction of the interference term. The classical period of these orbits near the 4/5 downhill bifurcation point ($\varepsilon = -2.475$) is approximately equal to the period of the $d4$ repetition, $(4.86)2\pi\bar{n}^3$, yielding $\gamma = 0.83$. The recurrence strength of each individual orbit will see a reduction in strength by this factor, but the interference term will be reduced by this factor squared, or 0.69.

Points C in Fig. 3 indicate a series of nonhydrogenic orbits, particularly in the 10 torr map. Here the mechanism is similar to the one proposed for the features at point B. For example, at $\varepsilon = -2.2$ near $\tilde{S} = 12$, we find a single strong peak in the 3 mtorr recurrence map and a series of weaker peaks between $\tilde{S} = 11.8$–12 in the 10 torr map. The primary hydrogenic contribution in this region is the 11/13 orbit ($\tilde{S} = 12.03$) with additional contributions from scattered combinations: $6/7 + 5/6$, $\tilde{S} = 12.025$; $7/8 + 4/5$, $\tilde{S} = 11.957$; $5/6 \times 2 + u$, $\tilde{S} = 11.953$ (among others). The combination $9/11 + u2$ is predicted to occur at a slightly lower scaled action, $\tilde{S} = 11.85$. In the unperturbed case, this collection of orbits is constructive around $\tilde{S} = 12$ and destructive near $\tilde{S} = 11.85$. In the perturbed case, with γ being approximately equal to 0.57 for any individual orbit, interference terms will be reduced by a factor of 3. With the lack of interference terms we can resolve three peaks in the 10 torr recurrence map, experimentally located at $\tilde{S} = 12.03$, 11.97, and 11.85, corresponding to the locations of the 11/13, $7/8 + 45$, and $9/11 + u2$ orbits, respectively. A similar instance where a single strong orbit appears to "decompose" into several weaker orbits occurs around the 9/11 hydrogenic orbit occurring near $\tilde{S} = 10$.

V. ENHANCED IONIZATION AND LOW ACTION RECURRENCES

There are other observed differences between the two experimental recurrence maps of Fig. 3 that are worthy of mention. One is the loss of recurrence strength beyond the ionization threshold ($\varepsilon = -2$), presumably due to the addition of new channels to ionization. For example, at $\varepsilon = -1.9$ (the highest fields attained with 10 torr), the peaks associated with the hydrogenic 7/9, $4/5 \times 2$, and $4/5 \times 3$ orbits (occurring at $\tilde{S} = 8$, 9.05, and 13.6, respectively) loose strength more quickly than similar orbits occurring at lower field strengths. For example, the 8/9 and 9/10 orbits, located at $\varepsilon = -2.6$, occur at similar actions and do not seem to lose significant recurrence strength. While the mechanism of collision-induced ionization is an attractive one, our current data, limited in field strength and lacking information in absolute normalization, are not enough to warrant further speculation.

Near the ionization threshold the density of classical orbits within the recurrence spectrum becomes particularly dense, and higher field strengths would make ionization effects both more apparent and simpler to analyze. Unfortunately, the threshold for gas discharge limited us to lower field strengths.

Another observation is the increase of recurrence strengths at scaled actions less than 1 in the 10 torr recurrence map. A significant fraction of this is due to contributions from the $5p_{1/2}$ series. We can simulate the contributions of the $5p_{1/2}$ series by taking the scaled-absorption spectra of both series in low gas environments, broadening them, and adding them together. The fabricated scaled-absorption spectrum is compared with the 10 torr spectrum to confirm the relative strengths of the two series prior to taking the Fourier transform. The fabricated recurrence spectrum does show actions at low frequency, but much lower in strength than that which is observed in the 10 torr recurrence map. We suspect that there are low action oscillations within the perturbed $5p_{3/2}$ series that act resonantly with the $5p_{1/2}$ series. These low action oscillations are likely due to coherent "combination" orbits formed by scattering off of a perturbing krypton atom (see Appendix). Due to the motion of the perturbing atom the coherency of these combinations is lost for longer period actions, but for shorter orbits these may be visible (see Appendix). One possible means for observing a two-center combination orbit is to perform a similar experiment using a laser-cooled perturbing gas. In such an environment the relative velocity of the Rydberg ion and the perturber would be reduced and would increase the coherence of the scattered combination. Additionally, the collisional deexcitation to the $5p_{1/2}$ series would be significantly reduced. In this environment the collisional perturbers would be essentially stationary, and the second Rydberg series would be eliminated.

VI. SUMMARY

We have adapted the techniques of recurrence spectroscopy to investigate the semiclassical dynamics of Rydberg electrons in a perturbing gas. The recurrence maps taken under conditions of low and high pressures of background gas illustrate the effects of collision-induced decoherence. We see these effects in the overall strength of recurrences as a function of scaled action and attribute this to collisionally induced decoherence and the subsequent inability of the returning wave function to interfere with itself. Our simple model of decoherence, applied to COT, is in general agreement with our observations. In addition, semiclassical orbits returning to the core interfere with one another, and we observe an apparent loss of orbit-orbit interference. Here we assert that the interference between orbits is more susceptible to decoherence in that the two returning wave fronts are both reduced to states of partial coherence. This manifests itself with the increase in recurrence strength for orbits that would otherwise be mutually destructive. Anomalously high recurrence strengths found at very low scaled actions suggests that coherent electron-perturber-ion orbits may be present, but interference of a second Rydberg series makes this difficult to confirm. Future studies involving a bath of ultracold perturbers may more clearly reveal semiclassical orbits with two scattering centers. Additionally, molecular perturbers should reveal inelastic collisions that connect classical orbits across different scaled energies.

APPENDIX: COHERENTLY SCATTERED COMBINATION ORBITS

While we are primarily focused on looking for decoherence effects, a Rydberg system surrounded by a relatively high-pressure environment presents a unique testing ground for ion-electron-atom interactions. An electron could, potentially, be scattered into a different trajectory altogether. For scaled energies above the ionization threshold a stable closed orbit can be scattered into an ionizing trajectory, fail to contribute to the regular interference oscillations at the core, and consequently fail to appear in the recurrence spectrum. Scattered electrons may be transferred to bound orbits that never return to the core and will also be unobservable in the recurrence spectrum. There is also the possibility of scattering an electron from one orbit to another bound, closed orbit. A collision between the Rydberg electron and the perturber may occur at any point within the trajectory. While it seems as if this would lead to an infinite number of incoherent "combination" orbits, there may be a finite number of important combination orbits of this type. Because of the short-range scattering potential the only way for an electron to transfer from one closed orbit to another is to have a scattering event occur at an intersection between two orbit paths. In addition, classical caustics cause the classical electron density to focus along certain points along the closed orbit path, making specific transfers much more likely than others. Finally, for such strange combination orbits to be observable in a recurrence spectrum the returning wave front must remain coherent over the time scale of the orbital period. For this to occur the motion of the perturber over the time scale of the orbital period must be significantly less than the wavelength of the Rydberg electron. For a single primitive orbit this condition is

$$\bar{v}_p \tau_{\mathrm{orb}} < \bar{\lambda}_e,$$
$$\tau_{\mathrm{orb}} < n/\bar{v}_p.$$

Under our current typical experimental conditions, the velocity of the perturber is about 1.6×10^{-4} a.u., $n = 55$, in which case the period of the combination orbit must be less than that of a primitive orbit period for it to be observable within the recurrence spectrum. While this has not been directly observed, the anomalously high strengths found at low action suggest that we may have contributions from such combination orbits. For an ultracold perturbing gas with velocities <1 m/s, decoherence due to the relative motion of the scattering centers would be negligible.

ACKNOWLEDGMENTS

We wish to acknowledge the National Science Foundation for support of this work.

[1] U. Eichmann, K. Richter, D. Wintgen, and W. Sandner, Phys. Rev. Lett. **61**, 2438 (1988).
[2] M. L. Du and J. B. Delos, Phys. Rev. A **38**, 1896 (1988).
[3] M. L. Du and J. B. Delos, Phys. Rev. A **38**, 1913 (1988).
[4] J. M. Mao and J. B. Delos, Phys. Rev. A **45**, 1746 (1992).
[5] J. Gao, J. B. Delos, and M. Baruch, Phys. Rev. A **46**, 1449 (1992).
[6] J. Gao and J. B. Delos, Phys. Rev. A **46**, 1455 (1992).
[7] M. Courtney, N. Spellmeyer, H. Jiao, and D. Kleppner, Phys. Rev. A **51**, 3604 (1995).
[8] J. Main, G. Wiebusch, K. Welge, J. Shaw, and J. B. Delos, Phys. Rev. A **49**, 847 (1994).
[9] M. L. Keeler and T. J. Morgan, Phys. Rev. A **59**, 4559 (1999).
[10] A. Kips, W. Vassen, W. Hogervorst, and P. A. Dando, Phys. Rev. A **58**, 3043 (1998).
[11] S. N. Pisharody, J. G. Zeibel, and R. R. Jones, Phys. Rev. A **61**, 063405 (2000).
[12] K. A. Bates, J. Masae, C. Vasilescu, and D. Schumacher, Phys. Rev. A **64**, 033409 (2001).
[13] M. S. Zhan, X. J. Liu, J. W. Cao, and J. P. Connerade, J. Phys. B **34**, 1175 (2001).
[14] S. Freund, R. Ubert, E. Flothmann, K. Welge, D. M. Wang, and J. B. Delos, Phys. Rev. A **65**, 053408 (2002).
[15] J. Murray-Krezan, J. Kelly, M. R. Kutteruf, and R. R. Jones, Phys. Rev. A **75**, 013401 (2007).
[16] D. Wang, Q. Xu, C. Yang, M. Wang, and X. Ma, J. Chem. Phys. **129**, 104310 (2008).
[17] M. L. Keeler, Phys. Rev. A **77**, 034503 (2008).
[18] J. D. Wright, H. Flores-Rueda, W. Huang, and T. J. Morgan, Phys. Rev. A **79**, 052510 (2009).
[19] J. D. Wright, J. M. DiSciacca, J. M. Lambert, and T. J. Morgan, Phys. Rev. A **81**, 063409 (2010).
[20] N. Spellmeyer, D. Kleppner, M. R. Haggerty, V. Kondratovich, J. B. Delos, and J. Gao, Phys. Rev. Lett. **79**, 1650 (1997).
[21] W. De-Hua, Commun. Theor. Phys. (Beijing, China) **49**, 467 (2008).
[22] E. Fermi, Nuovo Cimento **11**, 157 (1934).
[23] A. Omont, J. Phys. (Paris, France) **38**, 1343 (1977).
[24] N. Allard and J. Kielkopf, Rev. Mod. Phys. **54**, 1103 (1982).
[25] T. F. Gallagher, *Rydberg Atoms* (Cambridge University Press, Cambridge, UK, 1994).
[26] J. Main, G. Wiebusch, K. Welge, J. Shaw, and J. B. Delos, Phys. Rev. A **49**, 847 (1994).
[27] M. L. Keeler, Phys. Rev. A **76**, 052510 (2007).
[28] M. Courtney, H. Jiao, N. Spellmeyer, D. Kleppner, J. Gao, and J. B. Delos, Phys. Rev. Lett. **74**, 1538 (1995).
[29] H. A. Bethe and E. E. Salpeter, *Quantum Mechanics of One- and Two-Electron Atoms* (Plenum, New York, 1977).